Measurement of spin observables in neutron-proton elastic scattering

Part I: Correlation parameters

J. Arnold[2], B. van den Brandt[3], M. Daum[3], Ph. Demierre[1], M. Finger[4,5], M. Finger,Jr.[5], J. Franz[2], N. Goujon-Naef[1],
P. Hautle[3], R. Hess[1,a], A. Janata[5], J.A. Konter[3], H. Lacker[2], C. Lechanoine-Leluc[1], F. Lehar[6], S. Mango[3], D. Rapin[1],
E. Rössle[2], P.A. Schmelzbach[3], H. Schmitt[2], P. Sereni[2], M. Slunečka[4,5], A. Teglia[1,3] B. Vuaridel[1]

[1] DPNC, Université de Genève, 1211 Genève 4, Switzerland
[2] Fakultät für Physik der Universität Freiburg, 79104 Freiburg, Germany
[3] PSI, Paul-Scherrer-Institut, 5232 Villigen-PSI, Switzerland
[4] MFF, Karlova Universita, 18000 Praha, Czech Republic
[5] LNP, Joint Institute for Nuclear Research, 141980 Dubna, Russia
[6] DAPNIA/SPP, CEA/Saclay, 91191 Gif-sur-Yvette (CEDEX) France

Abstract. The spin correlation parameters A_{oonn}, A_{ooss}, A_{oosk}, A_{ookk} and the analyzing power A_{oono} have been measured in free np elastic scattering at kinetic energies of 260, 315, 380, 460 and 535 MeV in the c.m. angle range from $60°$ to $164°$. The experiment was performed at the Paul-Scherrer-Institut (PSI) using a polarized neutron beam with continuous energy incident on a polarized proton target. These data will contribute significantly to the determination of the isospin $I = 0$ nucleon-nucleon amplitudes.

1 Introduction

The scattering of two nucleons is one of the basic processes necessary to understand nuclear forces. The nucleon spin plays an important role in the hadronic interaction but, at present, all general theories fail to predict spin observables in any of the nucleon-nucleon scattering channels.

The scattering matrix used to describe nucleon-nucleon interaction is not directly measurable by experiment. If parity conservation, the generalized Pauli principle, and time reversal invariance are assumed, there are five isospin $I = 1$ and five $I = 0$ complex amplitudes characterising the scattering matrix. An unambiguous determination of these amplitudes requires the measurement of at least ten spin observables for each of pp and np scattering. A direct experimental reconstruction of the scattering matrix is the only means of providing complete information about the nucleon-nucleon interaction in a model-independent way.

In the years 1975-1985 a large world-wide experimental effort provided a complete and precise set of data in pp elastic scattering. A direct reconstruction of the scattering matrix was made for the first time in 1981 by the Geneva group [1]. Similar reconstructions have been subsequently performed and at present the $I = 1$ amplitudes are fairly well known up to 2.7 GeV [2].

Since 1985, a similar effort has been undertaken in the study of the np elastic scattering at all accelerators where

a beam of polarized neutrons was available, i.e. TRIUMF (200-500 MeV), LAMPF (480-800 MeV), SATURNE II (800-1100 MeV). Our experimental program at PSI (200-560 MeV) started in 1991. It has been directed specifically to the extension of the knowledge of the $I = 0$ nucleon-nucleon amplitudes at kinetic energies below 500 MeV. A very intense beam of polarized neutrons has been built, with the polarization orientable in any direction. A double-scattering experiment has been performed using a polarized proton target and a polarimeter to analyze the final polarization of recoil protons. This experiment allowed us to measure a large variety of spin observables, including several three-index parameters which have been measured for the first time in this energy range.

Throughout the paper, we use the formalism and the four-index notation for observables given in ref. [3], where the subscripts of any observable, X_{srbt}, refer to the polarization orientation of the scattered(s), recoil(r), beam(b), and target(t) particles, respectively. Each index (s, r, b, t) can take on the values k, n, s or 0 according to the particle polarization orientation in its attached laboratory frame. The direction $\hat{k}$ is defined as being along the particle trajectory, $\hat{n}$ along the normal to the scattering plane and $\hat{s}$ is orthogonal to the other two axes $(\hat{n} \times \hat{k})$. The 0 index stands for an unpolarized state.

This paper presents the results for the analyzing power A_{oono} as well as the spin correlation parameters A_{oonn}, A_{ookk}, A_{ooss} and A_{oosk}, the last two being measured as lin-
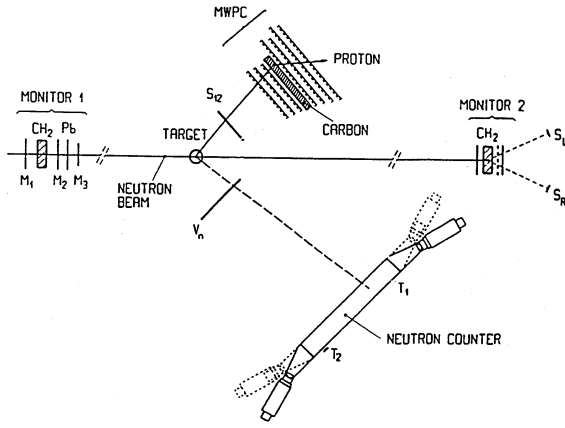

Fig. 1. Lay-out of the experimental set-up

ear combinations. These measurements were the basis of a Ph.D. thesis [4], where additional details may be found. The parameters including the measurements of the recoil proton polarization will be presented in a separate article [5]. Results for spin-transfer parameters measured with an unpolarized target are already published [6].

2 Experimental apparatus

The experimental setup is shown in Fig. 1. A detailed description of the polarized nucleon facility at PSI can be found in [7]. The apparatus and the experimental method used in the present measurements are essentially the same as described earlier [6]. In the following, only a summary of the most essential elements is presented, with emphasis on the polarized target.

2.1 Polarized neutron beam

The polarized neutron beam was created in the charge exchange reaction $C(\mathbf{p}, \mathbf{n})X$ at $0°$ using a polarized proton beam with an energy of 590 MeV and an intensity of $10\mu A$ incident on a carbon target. The produced neutrons had a continuous energy spectrum, consisting of a quasi-elastic peak around 530 MeV, and a broad continuum at lower energies.

It was found [8] that the polarization transfer at forward angles was most efficient via the $K_{ok''ko}$ polarization transfer mechanism. A longitudinally polarized neutron beam was produced by bombarding the carbon target with longitudinally polarized protons. The neutron beam polarization, P_B, which depends on the energy, was determined in a dedicated measurement [9]. For a typical proton beam polarization of 75%, the neutron beam polarization varied from 17.4% at 260 MeV to 44.7% at 535 MeV. The beam polarization was reversed every second.

Downstream of the production target, a combination of dipole magnets allowed rotation of the neutron spin from the longitudinal to the vertical or sideways directions; this process is energy dependent, therefore the beam polarization components were not the same for all energies.

The intensity of a few 10^6 neutrons s^{-1} cm^{-2}, the orientation of the polarization and the profile of the neutron beam have been continuously monitored and recorded during data taking by means of three monitoring devices. The first monitor (Monitor 1, Fig. 1) was located in the beam line and provided a relative measurement of the neutron intensity. It consisted of a 12 mm thick polyethylene target (CH$_2$) for conversion of neutrons into charged particles, and three 6 mm thick plastic scintillator detectors M_1, M_2 and M_3 [9]. The detector M_3 was also used as a veto counter in the np scattering trigger. A second device (Monitor 2, Fig. 1) was located downstream of the polarized target and was used to monitor the neutron beam profile as well as the orientation of the polarization. It consisted of a 1 cm thick CH$_2$ target to convert incoming neutrons to outgoing protons via (n, p) reactions, vertical and horizontal strip hodoscopes each containing five scintillation counters to provide the neutron beam profile and four counters placed at scattering angles of $30°$ to measure left-right and up-down scattering asymmetries. These counters, 5 cm in diameter and 3 mm thick, were located 44 cm downstream of the CH$_2$ target. A third device consisting of four scintillation counters and a proton beam steering system was used to keep the neutron beam on its central trajectory [10].

2.2 Polarized proton target (PPT)

The polarized target [11] has been built to fulfil the requirements of the experiment: transverse and longitudinal direction of polarization, large probe volume, large unobstructed access for the observation of outgoing protons and neutrons. To achieve sizeable polarizations, a magnetic field with high homogeneity over the target volume is required, at odds with large magnet opening angles. For this reason a frozen spin target has been developed: high nuclear polarizations were achieved in a high homogeneity solenoid, then the polarization was frozen and maintained in a holding magnet with large acceptance but poor field homogeneity.

The target itself consisted of 100 cm^3 (a cylinder of 54 mm diameter and 44 mm height) of butanol (CH$_3$(CH$_2$)$_2$ CH$_2$OH) or pentanol (CH$_3$(CH$_2$)$_3$CH$_2$OH) droplets, about 2 mm in diameter, doped with EHBA-Cr^V. A fluorocarbon dummy target, mounted underneath the target cell, could be lifted into the beam for background measurements, without interrupting the operation of the dilution refrigerator.

The target was polarized by dynamic nuclear polarization (DNP) in a 2.5 Tesla superconducting solenoid ($\Delta B/B \simeq 1.7 \ 10^{-4}$ over 100 cm^3). The target polarization was then frozen by lowering the temperature to about 50 mK, the holding magnet system was energised and the polarization solenoid was de-energised and moved to a position where it did not obstruct the measurements. The holding magnet system, which was integrated in the target cryostat, consisted of a pair of superconducting Helmholtz coils and a pair of superconducting saddle coils providing respectively the vertical and horizontal 0.8 T holding fields
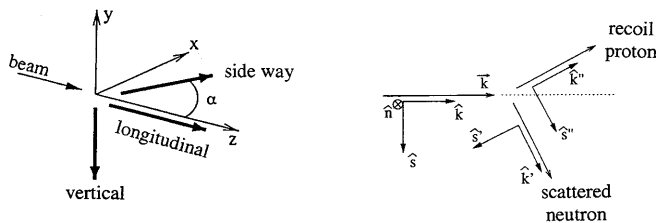
Fig. 2. a Directions of the target polarization used during the experiment; $\hat{x}$, $\hat{y}$, $\hat{z}$ is a right-handed system attached to the apparatus with $\hat{z}$ along the beam direction and $\hat{y}$ upwards. **b** Laboratory coordinate system $(\hat{s}, \hat{n}, \hat{k})$ attached to incident, scattered and recoil particles.

[7]. A linear combination of these fields, together with the rotatability of the cryostat around the vertical axis, allowed virtually any polarization direction with respect to the beam.

The polarization was measured by the method of nuclear magnetic resonance (NMR) with a relative precision between 3 and 4%. The polarization was reversed by DNP and not by reversing the holding field. Typical target polarizations (P_T) obtained during data taking ranged between 60% to 80% depending whether the polarization was parallel (P_T^+) or anti-parallel (P_T^-) to the holding field (in fact $P_T^- > P_T^+$). For each experimental period, two measurements of the polarization were performed, one at the beginning and one at the end of the period, i.e before going into and after coming out of frozen spin mode. An exponential interpolation between these two values gave the polarization at any time. Polarization relaxation times were longer than 1000 h at a temperature of $\leq$ 70 mK in a holding field of 0.8 T.

During the experiment, three orientations of the holding field were used as shown in Fig. 2a: 1) vertical, perpendicular to the beam axis, in the down direction; 2) horizontal, parallel to the beam axis; 3) horizontal, rotated by an angle of 56.5° with respect to the beam direction since a full 90° rotation is not possible because of the saddle coils.

2.3 Detection system

The experimental arrangement, shown in Fig. 1, has been built around the polarized target, allowing the detection of both the scattered neutron and the recoil proton. The neutron detector consisted of a wall of 11 plastic scintillator bars ($1300 \times 80 \times 200$ mm^3) mounted horizontally and placed 2.3 m from the center of the polarized target. An additional scintillation counter ($450 \times 300 \times 5.5$ mm^3), V_n in Fig. 1, placed between the hodoscope and the target was used to veto charged particles in the neutron detection system. Recoil protons were detected by multi-wire proportional chambers (MWPC) [12] placed on either side of a secondary carbon target. Between the MWPCs and the polarized target, a scintillation counter S_{12} (see Fig. 1) acted as a start counter for the entire acquisition system and was used for time-of-flight measurements.

A detailed description of the neutron counters can be found in [13]. The scintillation light was collected from each end of the bar by a XP2040 photomultiplier (PM) via a plexiglas light guide inclined at 15°. The horizontal coordinate of the neutron was deduced from the difference of the light arrival times at the two photomultipliers [6]. Two vertical scintillators (T_1 and T_2), placed behind the neutron hodoscope, were used to calibrate the reconstructed horizontal positions and the relative timing offsets of the bars.

Each MWPC consisted of two orthogonal sense planes, X and Y, 18 mm apart, with 20 μm tungsten wires spaced every 2 mm. The MWPCs were operated with the so-called magic gas mixture: 78.8% Argon, 14.2% Isobutane, 6.3% Methylal and 0.7% Freon. The high voltage, between 3600-3800 V, was applied separately to the X and Y parts of the chamber. Chambers of different sizes have been used: small (640×380 mm^2), medium (896×640 mm^2) and large (1024×640 mm^2). The distance between two chambers was 80 mm, and they were placed as shown in Fig. 1 in order to obtain optimal geometrical acceptance. Two platforms, which rolled on circular rails, were used to install these detectors at the proper position.

The trigger was realized using mainly ECL electronics, and allowed flexible programmability of the triggering conditions. Signals involved in the trigger decision come from the scintillation counters M_3, V_n, S_{12} and from the neutron counter. The logical combination which defined the trigger was done in a Programmable Logic Unit (PLU). Two trigger types have been used:

- np scattering: $\overline{M_3} \cdot \overline{V_n} \cdot S_{12} \cdot N$, for normal acquisition
- Gamma: $M_3 \cdot S_{12}$, used for time-of-flight calibration (see Sect. 3.3)

During the np scattering data taking, the trigger was changed to the "gamma" configuration for 10 msec every second.

The carbon scatterer between the MWPCs, which is used to analyze the scattered proton polarization [5], was not needed for the present experiment. However it was left in for the data taking in order to keep only the events for which the recoil proton had enough energy to penetrate the carbon target.

2.4 Data taking conditions

In order to cover a large angular range, measurements have been made at two different angular settings, called "A" and "B". The angular range covered in the centre-of-mass system was 60°-164°, with an overlap of 20° between the two positions.

In order to measure the four spin correlation parameters, the following four different beam/target polarization orientations were chosen: 1) for A_{oonn}, vertical beam and target orientation; this experimental condition will be referred to as $(\mathbf{y}, \mathbf{y})$; 2) for A_{ookk}, longitudinal beam and target orientations; this condition will be referred to as $(\mathbf{z}, \mathbf{z})$; 3) for A_{ooss} and A_{oosk} it was not possible to measure exclusively one of them separately. So we chose to measure

them twice with different mixture conditions referred to as (**x,xz**) and (**x,z**). These four beam/target conditions are shown in Table 1.

Since the sign of the target polarization was reversed about every two days and the sign of the beam polarization every second, we have measured elastic events for each of these four beam/target polarization orientations, i.e. $P_B^+ P_T^+$, $P_B^+ P_T^-$, $P_B^- P_T^+$, $P_B^- P_T^-$ in order to reduce possible systematic errors.

3 Off-line data analysis

The event reconstruction and the analysis have been performed in successive steps:

1. Tapes were read and decoded, some physical quantities were calculated and a preliminary event selection was made. Accepted events were written on new tapes, called summary tapes, containing the initial information and the reconstructed quantities.
2. Summary tapes were read, some physical quantities were re-calculated with higher precision and final cuts were made. Useful quantities were summed and recorded into sum-files.
3. Sum-files were used to calculate asymmetries and to extract the spin observables.

3.1 Event reconstruction

The neutron trajectory was obtained by considering the straight line joining the target center to the hit point of the neutron counter (Fig. 1). The vertical coordinate of the hit point was given by the center of the bar in which the signal was produced. The horizontal coordinate was calculated from the difference between the TDC signals of the two PMs at the ends of the hit bar.

The proton trajectory was calculated using the coordinates of hit wires in the first three multi-wire proportional chambers. Coordinates were corrected for misalignments of the MWPCs, measured using straight-track calibration data [6].

Since the magnetic field in the polarized target affected the proton trajectory, the measured proton angles needed to be corrected to obtain the true scattering angle. An iterative procedure has been used because the observed proton angle and the incident neutron energy are kinematically correlated. In our case, we did not have an independent measure of the proton energy; it was inferred from the proton angle. A tracking program has been employed to generate a correction table. Outgoing proton trajectories were computed from the scattering vertex through the detector planes according to the geometry of our setup. All materials traversed by the particles were considered and the corresponding energy losses and multiple scattering were taken into account. Since we did not have a precise knowledge of the scattering vertex, an average path in the target was taken. Resulting corrections were below 2°.
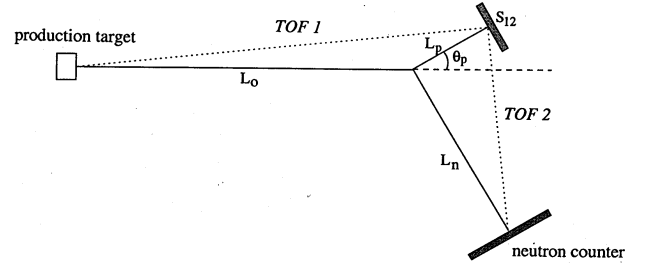

Fig. 3. Time-of-flight measurements for the calculation of the incident neutron energy

3.2 Definition of coordinate axes and scattering angles

The unit vectors are shown in Fig. 2b. The laboratory scattering angles have been calculated as follows:

$$\text{Neutron} \rightarrow \hat{n}_{(n)} = \frac{\mathbf{k} \times \mathbf{k}'}{|\mathbf{k} \times \mathbf{k}'|}, \ \cos\theta_n = \hat{k} \cdot \hat{k}',$$

$$\cos\phi_n = \hat{n}_{(n)} \cdot \hat{y}, \ \sin\phi_n = -\hat{n}_{(n)} \cdot \hat{x}$$

$$\text{Proton} \rightarrow \hat{n}_{(p)} = -\frac{\mathbf{k} \times \mathbf{k}''}{|\mathbf{k} \times \mathbf{k}''|}, \ \cos\theta_p = \hat{k} \cdot \hat{k}'',$$

$$\cos\phi_p = \hat{n}_{(p)} \cdot \hat{y}, \ \sin\phi_p = -\hat{n}_{(p)} \cdot \hat{x}$$

where $\hat{x}, \hat{y}, \hat{z}$ is a right-handed system attached to the apparatus with $\hat{z}$ along the beam direction and $\hat{y}$ upwards. Note that in our experimental set-up the proton detector is on the left and the neutron counter is on the right, with respect to the beam direction. Our definition agrees with the Basle convention [14]. With these definitions, the two normals, $\hat{n}_{(p)}$ and $\hat{n}_{(n)}$, must coincide within the experimental error for coplanar events and $\phi_p = \phi_n$ for later convenience in the analysis.

Both neutron and proton polar lab-angles were used to calculate $\theta_n^{c.m.}$ and $\theta_p^{c.m.}$ from which we made the weighted averages to improve the precision

$$\Theta_{c.m.} = \frac{\theta_n^{c.m.}/\sigma_{\theta_n}^2 + (180^o - \theta_p^{c.m.})/\sigma_{\theta_p}^2}{1/\sigma_{\theta_n}^2 + 1/\sigma_{\theta_p}^2} \quad \text{and}$$

$$\phi_{c.m.} = \phi = \frac{\phi_n/\sigma_{\phi_n}^2 + \phi_p/\sigma_{\phi_p}^2}{1/\sigma_{\phi_n}^2 + 1/\sigma_{\phi_p}^2}, \quad (1)$$

where σ_{ϕ_n}, σ_{ϕ_p}, σ_{θ_n} and σ_{θ_p} are the neutron and proton angle resolutions.

3.3 Incident neutron energy

Neutrons were produced as secondary particles by proton-nucleus collisions and hence had a broad momentum distribution. The momentum of the incident neutron had to be determined from the kinematics of each single event by the time-of-flight (TOF) method. We did not have direct access to the incident neutron time-of-flight (TOF_0), however it could be derived from the TOF_1 measured between the counter S_{12} and the 50 MHz signal coming from the accelerator which represents the proton bunch

arrival at the production target as shown in Fig. 3. We have $TOF_0 = TOF_1 - TOF_p$ where $TOF_p = L_p/v_p$, L_p is the distance of the S_{12} counter from the center of the polarized target and v_p is the proton velocity. To obtain a first estimate of the neutron velocity v_0, we assumed that $v_p = v_0 \cos\theta_p$, so that

$$v_0 = \frac{L_0 + L_p/\cos\theta_p}{TOF_1}. \quad (2)$$

An iterative procedure started from this value to calculate the true neutron velocity. Using v_0 and θ_p, the correction of the magnetic field effect of the polarized target was performed and the kinematics of the reaction calculated. From the proton energy and taking into account the energy loss, we obtained TOF_p, which allowed to calculate more and more precise values of v_0, until convergence was obtained.

The bunched structure of the neutron beam was the cause of an ambiguity in the energy reconstruction. Indeed, fast neutrons could be simulated by slow neutrons from the preceding bunch. The time-of-flight, TOF_1, was in fact known up to an additive term, $n \cdot \Delta$, where $\Delta = 19.75$ ns is the time between two consecutive bunches and n an integer number. To eliminate this ambiguity, we rejected events coming from slow incident neutrons by a second, independent time-of-flight measurement, TOF_2, which was the difference between the times-of-flight of the scattered neutron and the recoil proton.

Calibration of the TOF_1 measurement was made using γ's produced in the decays of π^o particles coming from the neutron production target [6]. They are converted into electrons in the M_3 counter. We collected calibration data during all data taking periods with the trigger configuration described in Sect. 2.3.

3.4 Kinematic cuts

In order to select elastic events, we took advantage of their geometrical features: trajectories had to lie in the same plane and the angle between the scattered neutron and the recoil proton was determined by kinematics. We controlled this by considering the distributions of

$$\phi_{diff} = \phi_n - \phi_p \qquad \text{and} \qquad \theta_{open} = \theta_n + \theta_p \quad (3)$$

Since θ_{open} is energy dependent, we have considered

$$\theta_{diff} = \theta_n^{c.m.} - (180^o - \theta_p^{c.m.}) \quad (4)$$

which is an energy-independent value and whose distribution is centred around zero. In the final analysis we rejected events having either of these two quantities farther than 3σ from the centre of the distributions.

At the end of the reconstruction, we retained 24% of the recorded events. The same reconstruction procedure had been performed for background data and events were subjected to the same selection criteria.

4 Extraction of spin observables

4.1 General formulae

When the polarization of the outgoing particles is not analyzed, the cross section of the reaction $\mathbf{np} \to np$ is given, at fixed kinetic energy E of the incident neutron, by the spin-dependent expression

$$\frac{d\sigma}{d\Omega}(E, \Theta_{c.m.}, \phi)$$
$$= I_{oooo}\left\{1 + P_B(\hat{P}_B \cdot \hat{n})A_{oono}\right.$$
$$\left. + P_T(\hat{P}_T \cdot \hat{n})A_{ooon} + P_B P_T A_{oopq}\right\}, \quad (5)$$

where

$$A_{oopq} = (\hat{P}_B \cdot \hat{n})(\hat{P}_T \cdot \hat{n})A_{oonn} + (\hat{P}_B \cdot \hat{s})(\hat{P}_T \cdot \hat{s})A_{ooss}$$
$$+ (\hat{P}_B \cdot \hat{k})(\hat{P}_T \cdot \hat{k})A_{ookk}$$
$$+ \left((\hat{P}_B \cdot \hat{s})(\hat{P}_T \cdot \hat{k}) + (\hat{P}_B \cdot \hat{k})(\hat{P}_T \cdot \hat{s})\right)A_{oosk}. \quad (6)$$

Here, I_{oooo} is the unpolarized cross section, P_B and P_T are the beam and target polarization, $\hat{P}_B$ and $\hat{P}_T$ are the corresponding unit vectors. We have chosen a convention such that the unit vectors do not change sign between beam/target $+$ or $-$ but the sign manifests itself on P_B and P_T.

The total number of measured events is related to the cross section by

$$N(E, \Theta_{c.m.}, \phi) = \frac{d\sigma}{d\Omega}(E, \Theta_{c.m.}, \phi)\, \eta(E, \Theta_{c.m.}, \phi)\, L, \quad (7)$$

where η is the detection efficiency of our experimental apparatus and L is the luminosity, a factor including the incident beam intensity, the target density and the measurement duration. The acceptance and efficiency of the two data sets with opposite beam polarization(P_B^+, P_B^-) can be considered to be equal, because they have been recorded while flipping the beam polarization every second. This is not true for the two data sets with opposite target polarization, (P_T^+, P_T^-) because many hours (even days) could have gone by between the two measurements. Therefore, we calculated the rate asymmetries separately for each target polarization $\epsilon^{(P_T^+)}$ and $\epsilon^{(P_T^-)}$ from beam polarization $+$ and $-$:

$$\epsilon = \frac{N^{(P_B^+)} - N^{(P_B^-)}}{N^{(P_B^+)} + N^{(P_B^-)}}. \quad (8)$$

The counts N are normalized to the corresponding counts in the Monitor 1, proportional to the integrated luminosity L of the measurement, thereby eliminating the dependence on efficiency, luminosity and the I_{oooo} parameter. The asymmetry becomes

$$\epsilon = |P_B|\frac{(\hat{P}_B \cdot \hat{n})A_{oono} + P_T A_{oopq}}{1 + P_T(\hat{P}_T \cdot \hat{n})A_{ooon}} \quad (9)$$

where we have supposed that the beam polarizations are equal in the two states: $|P_B^+| = |P_B^-| \equiv |P_B|$. Since from the generalized Pauli principle $A_{oono} = A_{ooon}$, only two unknown quantities are present in (9), A_{oono} and A_{oopq}, which can be extracted separately.

Practically, from data taken with both beam and target polarizations $\hat{y}$-oriented, two parameters could be extracted, namely A_{oonn} and the 1-spin parameter A_{oono} ($= A_{ooon}$). But when analyzing data with beam and target polarizations different from the $\hat{y}$-orientation, the coefficient multiplying the one-spin parameter is close to zero, and the solution for the observables is delicate. Therefore, in this case we have fixed the A_{oono} values to PSA predictions [15] and determined the A_{oopq} only.

From the two measured asymmetries, $\epsilon^{(P_T^+)}$ and $\epsilon^{(P_T^-)}$, we obtained A_{oopq} with redundancy ($A_{oopq}^{(P_T^+)}$ and $A_{oopq}^{(P_T^-)}$). This redundancy was used to check the consistency of the results and deduce normalization uncertainties as discussed in Sect. 4.5.

Since the renormalization discussed after (8) is small ($< 10^{-2}$), the statistical errors for the measured asymmetries ϵ are well approximated by

$$\sigma_\epsilon^2 = \frac{1 - \epsilon^2}{N^{(P_B^+)} + N^{(P_B^-)}} \qquad (10)$$

from which errors on the derived quantities A_{oopq} (and A_{oono} when possible) have been calculated.

4.2 Coefficients determination

The terms multiplying A_{oono} and A_{ooon} (see (5)), as well as those of the linear combination A_{oopq} (see (6)), can be developed by expressing $\hat{s}$, $\hat{n}$, $\hat{k}$ and $\hat{P}_B$ and $\hat{P}_T$ in the laboratory frame ($\hat{x}, \hat{y}, \hat{z}$):

$$\begin{aligned} \hat{s} &= (\ \cos\phi,\ \sin\phi, 0\ ) \\ \hat{n} &= (-\sin\phi, \cos\phi, 0\ ) \quad \text{and} \quad \begin{aligned} \mathbf{P}_B &= P_B \cdot (\ b_x, b_y, b_z\ ) \\ \mathbf{P}_T &= P_T \cdot (\ t_x, t_y, t_z\ ). \end{aligned} \\ \hat{k} &= (\quad 0,\qquad 0,\ 1\ ) \end{aligned}$$

$$(11)$$

We then obtain for (5)

$$\begin{aligned} (\hat{P}_B \cdot \hat{n}) &= b_y \cos\phi - b_x \sin\phi \\ (\hat{P}_T \cdot \hat{n}) &= t_y \cos\phi - t_x \sin\phi \end{aligned} \qquad (12)$$

and for (6)

$$\begin{aligned} (\hat{P}_B \cdot \hat{n})(\hat{P}_T \cdot \hat{n}) \\ = b_x t_x \sin^2\phi + b_y t_y \cos^2\phi - (b_x t_y + b_y t_x)\sin\phi\cos\phi \end{aligned}$$

$$\begin{aligned} (\hat{P}_B \cdot \hat{s})(\hat{P}_T \cdot \hat{s}) \\ = b_x t_x \cos^2\phi + b_y t_y \sin^2\phi + (b_x t_y + b_y t_x)\sin\phi\cos\phi \\ (\hat{P}_B \cdot \hat{k})(\hat{P}_T \cdot \hat{k}) = b_z t_z \\ (\hat{P}_B \cdot \hat{s})(\hat{P}_T \cdot \hat{k}) + (\hat{P}_B \cdot \hat{k})(\hat{P}_T \cdot \hat{s}) \\ = b_x t_z \cos\phi + b_y t_z \sin\phi + b_z t_x \cos\phi + b_z t_y \sin\phi. \quad (13) \end{aligned}$$

All these coefficients have been calculated as follows:

1) The target polarization components (t_x, t_y, t_z) have been defined for the three different orientations of the PPT holding field. The sideways target polarization orientation was at $56.5°$ with respect to the z-axis, so in this case, a longitudinal component was present.

2) The beam polarization components (b_x, b_y, b_z) have been calculated for the three different beam polarization orientations (see Sect. 2.1). The effect of the PPT holding field has also been taken into account.

3) In order to estimate the effect of the finite ϕ range acceptance (depending on $\Theta_{c.m.}$) without binning in ϕ, we have accumulated sums during the off-line event selection into sum-files, providing for each bin ($E, \Theta_{c.m.}$) the average values of $\langle \sin\phi \rangle$, $\langle \cos\phi \rangle$, $\langle \sin\phi\cos\phi \rangle$, $\langle \sin^2\phi \rangle$, $\langle \cos^2\phi \rangle$.

4.3 Extraction of the results

We could have simply used these calculated coefficients to extract the physics results. But this would have provided A_{pq}^{mes} results containing an angle-dependent linear combination of spin-correlation parameters different for each incident energy(E). We therefore corrected the measured A_{pq}^{mes} in order to keep only the most dominant terms, which is equivalent to putting $\phi = 0$ (see (13)). The terms with small coefficients (i.e those containing $\sin(\phi)$) were alculated and multiplied by the corresponding spin-correlation parameter obtained from PSA predictions [15] and subtracted from the measured A_{pq}^{mes} such that

$$\begin{aligned} A_{pq}^{mes}(\phi = 0) \\ = \langle A_{pq}^{mes}(\phi) \rangle - (\langle A_{pq}^{PSA}(\phi) \rangle - \langle A_{pq}^{PSA}(\phi = 0) \rangle). \quad (14) \end{aligned}$$

These corrections were very small and never larger than $1.3\ \sigma_{stat}$. For the four different beam/target type measurements ($\mathbf{y}, \mathbf{y}$), ($\mathbf{z}, \mathbf{z}$), ($\mathbf{x}, \mathbf{xz}$) and ($\mathbf{x}, \mathbf{z}$) as defined in Sect. 2.4, one can say:

1) For the ($\mathbf{y}, \mathbf{y}$) measurement, we end up with a pure A_{oonn} measurement at all angles and energies. The contribution from A_{ooss} which contains a $\sin^2\phi$ term has been subtracted from the measured A_{pq}^{mes} leaving results containing only A_{oonn}. The beam polarization had an energy-dependent longitudinal component (see Sect. 2.1) which would only enter via the parameter A_{ookn} which is identically zero due to parity conservation. All the physics effects depended only on the vertical polarization of the beam.
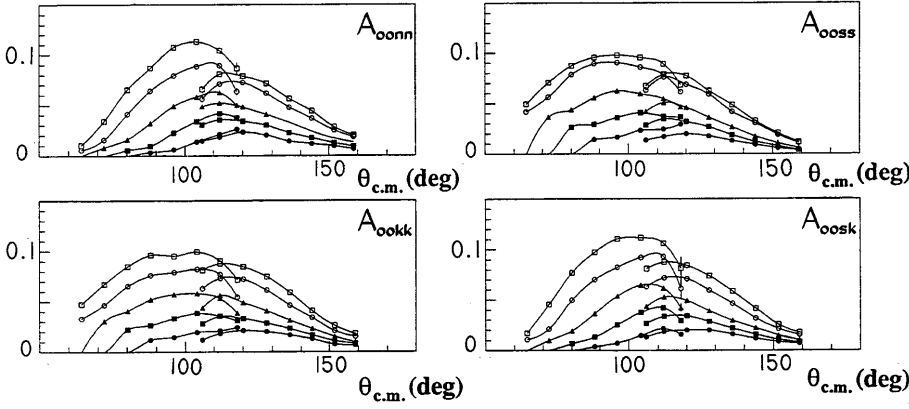
Fig. 4. Dilution factors for the four spin correlation parameters. Curves are guides for the eyes, connecting points at the same energy: 260 MeV (smallest dilution factor shown as black dots), 315 MeV, 380 MeV, 460 MeV and 535 MeV (largest dilution factor shown as open squares)

Table 1. Values of the coefficients for the linear combinations of the spin correlation parameters in the A_{oopq} measurements for the four different beam and target polarization orientations. For the $(\mathbf{z}, \mathbf{z})$ and $(\mathbf{y}, \mathbf{y})$ configurations, the coefficients are identical for all incident kinetic energies

P_B	P_T	A_{oonn}	A_{ooss}	A_{oosk}	A_{ookk}	$T_{kin}[MeV]$
$\mathbf{z}$	$\mathbf{z}$	0	0	0	1	all
$\mathbf{y}$	$\mathbf{y}$	1	0	0	0	all
$\mathbf{x}$	$\mathbf{xz}$	0	- 0.769	0.185	0.214	260
		0	- 0.802	0.303	0.151	315
		0	- 0.822	0.400	0.095	380
		0	- 0.831	0.483	0.045	460
		0	- 0.834	0.537	0.010	535
$\mathbf{x}$	$\mathbf{z}$	0	0	0.922	0.388	260
		0	0	0.962	0.273	315
		0	0	0.985	0.172	380
		0	0	0.997	0.081	460
		0	0	0.999	0.018	535

2) For $(\mathbf{z}, \mathbf{z})$ measurement, we have measured pure A_{ookk}. No corrections were needed there.

3) For the $(\mathbf{x}, \mathbf{xz})$ and $(\mathbf{x}, \mathbf{z})$, we end up with a linear combination of two or three coefficients. The combination is different for each energy, but stays the same at all angles.

Table 1 summarizes the measured linear combination for the four measurements performed under conditions $(\mathbf{y}, \mathbf{y})$, $(\mathbf{z}, \mathbf{z})$, $(\mathbf{x}, \mathbf{xz})$ and $(\mathbf{x}, \mathbf{z})$ as discussed above. We observe in Table 1 that A_{oonn} and A_{ookk} are pure spin correlation parameters, whereas for A_{ooss} and A_{oosk} a mixture is always present. The latter two parameters can be extracted using the appropriate linear combinations for each energy in the measured A_{oopq} as given in Table 1.

4.4 Background subtraction

The background effect can be considered as a dilution of the proton polarization contribution to the differential cross section
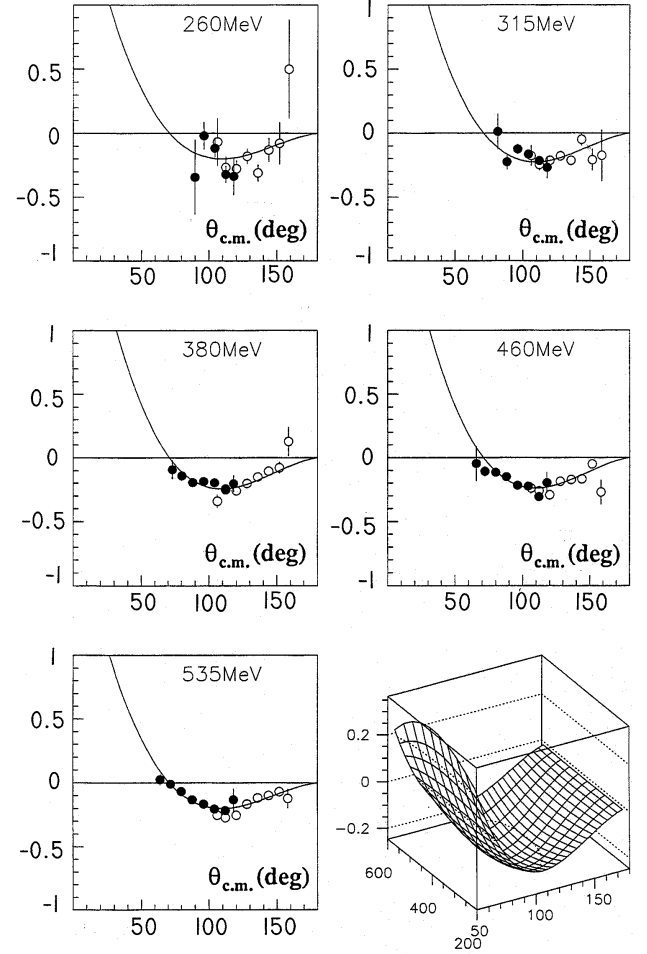
Fig. 5. Background asymmetry A_{bg}. Black dots correspond to arm position "A", open circles to arm position "B". The bottom right figure is a 3-dimensional representation of A_{bg} as a function of angle and incident kinetic energy

$$(1 - f) \left\{ \begin{matrix} \text{proton} \\ \text{contribution} \end{matrix} \right\} + f \left\{ \begin{matrix} \text{background} \\ \text{contribution} \end{matrix} \right\}$$

where the dilution factor f can be estimated as the ratio between the number of events recorded with dummy

$$A_{ooon}$$
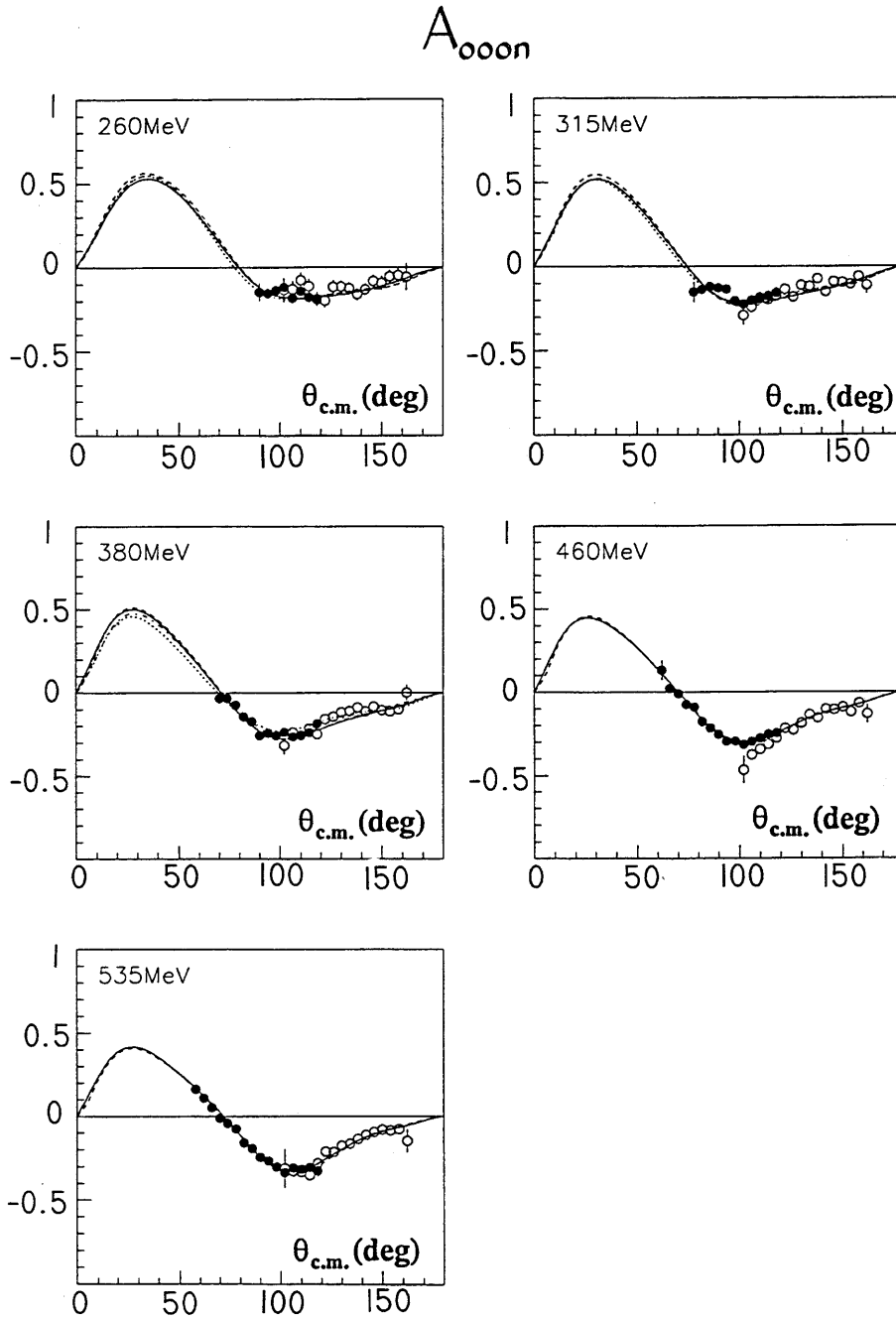
Fig. 6. Results for A_{ooon} as a function of $\Theta_{c.m.}$ and of the kinetic neutron energy. Black dots correspond to angular setting A, open circles to position B. The full line is a prediction from the PSA Saclay-Geneva [15], the dotted line from the Paris potential [17], the dashed line from VPI PSA [16] and the dashed-dotted line from the Bonn potential [18]

target (N_d) and with the polarized target (N). Dummy data have been normalized by matching the wings of the θ_{diff} distributions ((4)), supposing that the events in this region are only background events. Then:

$$f = \frac{N_d}{N}\frac{W}{W_d} \qquad (15)$$

where W and W_d are the number of events in the wings of the θ_{diff} distribution for normal and dummy target, respectively. The dilution factor, calculated for each $(E, \Theta_{c.m.})$ bin, has been found to be at most 0.11; its dependence on energy and scattering angle is shown in Fig. 4.

The differential cross section for scattering on the dummy target is a particular case of the general formula (5), with the target polarization P_T set to zero:

$$\frac{d\sigma}{d\Omega}(E, \Theta_{c.m.}, \phi)_{dummy} \quad \propto \quad 1 + P_B(\hat{P}_B \cdot \hat{n})A_{bg} \qquad (16)$$

where A_{bg} is the asymmetry parameter A_{oono} for the dummy scattering.

To measure A_{bg}, we have analyzed the dummy target data with beam polarization along the $\hat{n}$ direction and we have calculated the asymmetry, ϵ_d, of the observed number of events for polarizations up and down:
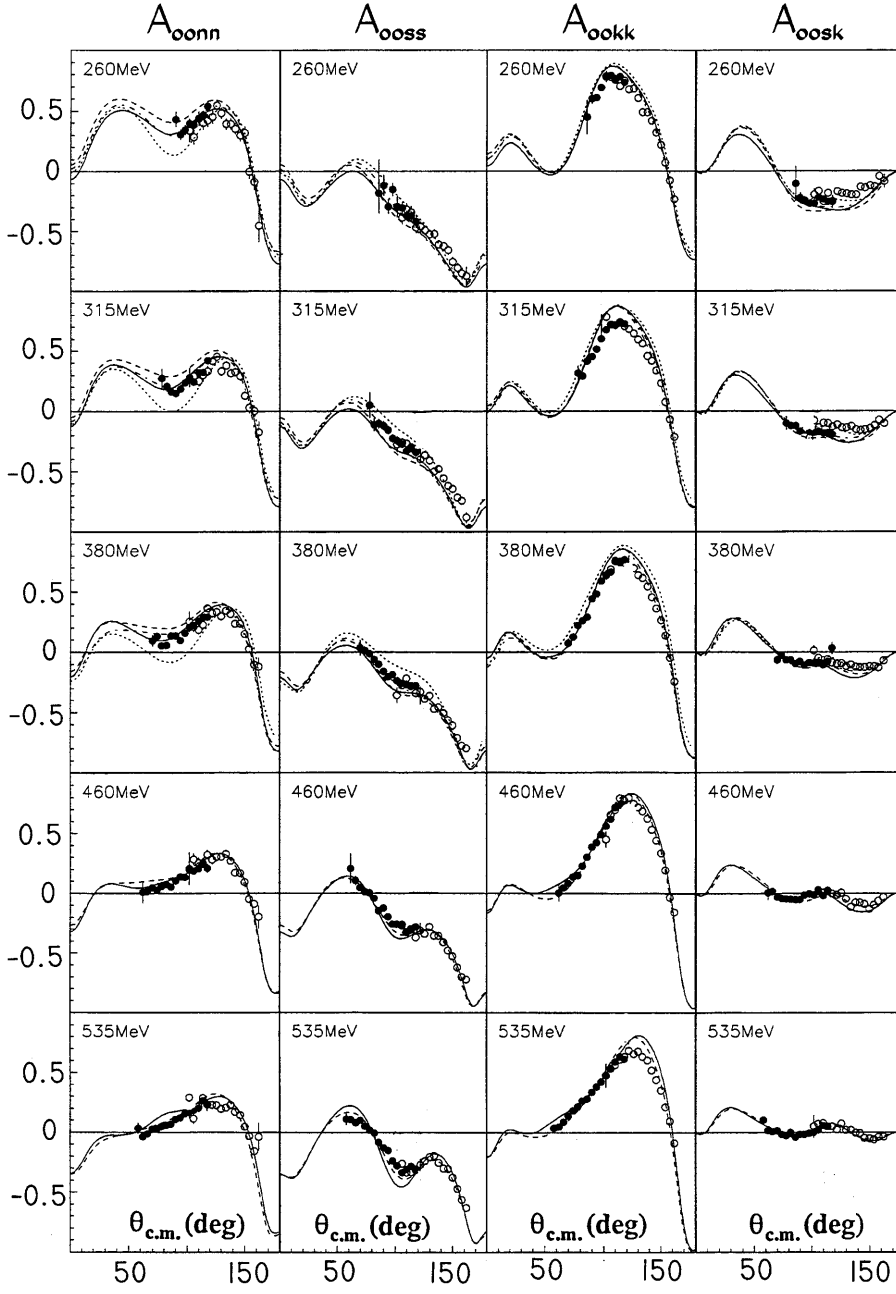
Fig. 7. Results for A_{oonn}, A_{ooss}, A_{ookk}, A_{oosk} as function of $\Theta_{c.m.}$ and of the kinetic neutron energy. The same symbols are used as in Fig. 6

$$\epsilon_d = \frac{N_d^{(P_B^+)} - N_d^{(P_B^-)}}{N_d^{(P_B^+)} + N_d^{(P_B^-)}} = P_B(\hat{P}_B \cdot \hat{n})A_{bg} \qquad (17)$$

from which A_{bg} can be derived. Results (Fig. 5) have been fitted by a two-dimensional function of the energy and the scattering angle. The A_{bg} parameter has been constrained to zero at 180° in the fit.

Taking into account the background effect, (5) becomes

$$\frac{d\sigma}{d\Omega}(E, \Theta_{c.m.}, \phi)$$

$$= \frac{I_{oooo}}{(1-f)}\left\{1 + P_B(\hat{P}_B \cdot \hat{n})\left[(1-f)A_{oono} + fA_{bg}\right]\right.$$

Table 2. a) Systematic errors on A_{oono}. Multiplicative global effects due to P_B uncertainties are included. b) Systematic errors on A_{oopq}. Multiplicative global effects due to P_B and P_T uncertainties are included

	260 MeV	315 MeV	380 MeV	460 MeV	535 MeV
a)	1.8 %	1.2 %	1.2 %	1.9 %	1.2 %
b)	3.9 %	3.7 %	3.7 %	4.0 %	3.7 %

$$\left. + P_T(\hat{P}_T \cdot \hat{n})(1-f)A_{ooon} + P_B P_T(1-f)A_{oopq}\right\} \quad (18)$$

from which the spin parameters have been extracted as described in the above section.

Table 3. Numerical values for the *np* elastic scattering spin observable A_{oono} as a function of $\Theta_{c.m.}$ and the neutron kinetic energy. The errors are purely statistical. The normalization errors due to the beam polarization are given in Table 2a)

	$\Theta_{c.m.}$ [°]	260 MeV	315 MeV	380 MeV	460 MeV	535 MeV
	58					0.159 ± 0.029
	62				0.128 ± 0.058	0.106 ± 0.011
	66				0.021 ± 0.019	0.051 ± 0.011
	70			-0.033 ± 0.032	-0.009 ± 0.015	-0.010 ± 0.012
	74			-0.032 ± 0.019	-0.072 ± 0.015	-0.041 ± 0.014
	78		-0.147 ± 0.058	-0.072 ± 0.016	-0.088 ± 0.016	-0.072 ± 0.016
	82		-0.132 ± 0.028	-0.140 ± 0.015	-0.171 ± 0.017	-0.154 ± 0.017
"A"	86		-0.116 ± 0.022	-0.167 ± 0.016	-0.208 ± 0.018	-0.185 ± 0.019
	90	-0.141 ± 0.052	-0.124 ± 0.021	-0.248 ± 0.017	-0.244 ± 0.019	-0.237 ± 0.020
	94	-0.149 ± 0.034	-0.131 ± 0.021	-0.234 ± 0.017	-0.284 ± 0.020	-0.258 ± 0.022
	98	-0.133 ± 0.032	-0.198 ± 0.021	-0.246 ± 0.018	-0.284 ± 0.021	-0.292 ± 0.023
	102	-0.115 ± 0.031	-0.215 ± 0.021	-0.229 ± 0.019	-0.302 ± 0.022	-0.325 ± 0.024
	106	-0.175 ± 0.029	-0.194 ± 0.021	-0.254 ± 0.019	-0.285 ± 0.022	-0.298 ± 0.024
	110	-0.137 ± 0.030	-0.186 ± 0.022	-0.246 ± 0.019	-0.267 ± 0.022	-0.306 ± 0.023
	114	-0.170 ± 0.029	-0.169 ± 0.022	-0.231 ± 0.019	-0.244 ± 0.022	-0.297 ± 0.023
	118	-0.178 ± 0.040	-0.151 ± 0.027	-0.179 ± 0.023	-0.236 ± 0.028	-0.315 ± 0.037
	102	-0.129 ± 0.071	-0.280 ± 0.054	-0.303 ± 0.055	-0.448 ± 0.080	-0.299 ± 0.116
	106	-0.124 ± 0.046	-0.232 ± 0.033	-0.228 ± 0.027	-0.362 ± 0.030	-0.318 ± 0.028
	110	-0.072 ± 0.047	-0.178 ± 0.031	-0.247 ± 0.026	-0.330 ± 0.028	-0.322 ± 0.026
	114	-0.108 ± 0.043	-0.189 ± 0.031	-0.207 ± 0.025	-0.301 ± 0.028	-0.340 ± 0.026
	118	-0.183 ± 0.041	-0.165 ± 0.030	-0.240 ± 0.025	-0.263 ± 0.028	-0.270 ± 0.026
	122	-0.192 ± 0.040	-0.131 ± 0.029	-0.152 ± 0.024	-0.210 ± 0.028	-0.205 ± 0.025
	126	-0.111 ± 0.040	-0.174 ± 0.028	-0.138 ± 0.023	-0.218 ± 0.026	-0.208 ± 0.024
"B"	130	-0.111 ± 0.038	-0.107 ± 0.026	-0.114 ± 0.021	-0.180 ± 0.025	-0.171 ± 0.023
	134	-0.119 ± 0.035	-0.114 ± 0.026	-0.106 ± 0.021	-0.131 ± 0.023	-0.159 ± 0.020
	138	-0.155 ± 0.035	-0.070 ± 0.025	-0.085 ± 0.020	-0.150 ± 0.021	-0.130 ± 0.020
	142	-0.127 ± 0.035	-0.143 ± 0.024	-0.109 ± 0.018	-0.098 ± 0.020	-0.106 ± 0.018
	146	-0.078 ± 0.037	-0.087 ± 0.024	-0.080 ± 0.019	-0.102 ± 0.019	-0.091 ± 0.017
	150	-0.090 ± 0.041	-0.091 ± 0.025	-0.102 ± 0.018	-0.088 ± 0.018	-0.078 ± 0.016
	154	-0.053 ± 0.039	-0.101 ± 0.027	-0.108 ± 0.019	-0.115 ± 0.019	-0.083 ± 0.016
	158	-0.046 ± 0.043	-0.057 ± 0.029	-0.097 ± 0.020	-0.066 ± 0.021	-0.076 ± 0.018
	162	-0.054 ± 0.078	-0.108 ± 0.053	0.000 ± 0.046	-0.128 ± 0.054	-0.141 ± 0.069

4.5 Systematic uncertainties

Consistency tests have been performed using data measured with a longitudinally polarized beam (i.e along $\hat{k}$). In this case the beam polarization direction is along $\hat{k}$ for all energies due to the way the polarized neutron beam has been produced (see Sect. 2.1). When measurements were performed with a longitudinally polarized target, one could access only one spin-dependent parameter, A_{ookk}, which was therefore measured twice, once with target polarization + (A^{+}_{ookk}) and once with target polarization − (A^{-}_{ookk}). A relative disagreement between the two measurements of 12% has been found. Intense investigation has been undertaken to understand the problem as detailed below:

1) It was found to be independent of the incident beam energy.

2) A vertical parasitic beam polarization component of 1.2% has been identified with the beam polarimeter. Therefore this vertical polarization cannot be induced by the target magnetic field since a sideway magnetic field would be required to turn a longitudinal polarization. This vertical beam component has also been independently observed from the dummy target data taken in the same period. This vertical polarization component could explain one third of the observed disagreement, and when averaging the two measurements with the two target orientations it should cancel.

3) A relative difference in target polarization between the upper and lower part of $(4 \pm 1)\%$ has been found

Table 4. Numerical values for the np elastic scattering spin-correlation observable A_{oonn} as a function of $\Theta_{c.m.}$ and the neutron kinetic energy. The errors are purely statistical. The normalization errors are given in Table 2b)

	$\Theta_{c.m.}$ [°]	260 MeV			315 MeV			380 MeV			460 MeV			535 MeV		
	58													0.033	±	0.047
	62										0.010	±	0.092	-0.039	±	0.018
	66										0.015	±	0.030	-0.016	±	0.018
	70							0.096	±	0.049	0.048	±	0.023	0.027	±	0.018
	74							0.133	±	0.028	0.026	±	0.023	0.029	±	0.018
	78				0.275	±	0.083	0.053	±	0.024	0.056	±	0.023	0.046	±	0.018
	82				0.206	±	0.041	0.056	±	0.023	0.074	±	0.024	0.059	±	0.019
"A"	86				0.164	±	0.031	0.135	±	0.023	0.053	±	0.024	0.067	±	0.019
	90	0.433	±	0.069	0.149	±	0.030	0.135	±	0.023	0.104	±	0.025	0.109	±	0.020
	94	0.306	±	0.047	0.187	±	0.029	0.099	±	0.023	0.137	±	0.025	0.119	±	0.021
	98	0.344	±	0.043	0.239	±	0.029	0.161	±	0.023	0.134	±	0.025	0.154	±	0.021
	102	0.399	±	0.040	0.265	±	0.028	0.207	±	0.023	0.195	±	0.025	0.169	±	0.022
	106	0.388	±	0.039	0.243	±	0.027	0.222	±	0.023	0.186	±	0.025	0.180	±	0.022
	110	0.440	±	0.036	0.324	±	0.027	0.259	±	0.022	0.206	±	0.024	0.202	±	0.022
	114	0.469	±	0.035	0.321	±	0.026	0.289	±	0.021	0.248	±	0.024	0.263	±	0.023
	118	0.539	±	0.048	0.421	±	0.034	0.292	±	0.028	0.209	±	0.038	0.228	±	0.050
	102	0.341	±	0.105	0.280	±	0.086	0.254	±	0.087	0.205	±	0.137	0.289	±	0.172
	106	0.286	±	0.068	0.291	±	0.050	0.209	±	0.042	0.283	±	0.048	0.114	±	0.045
	110	0.438	±	0.064	0.253	±	0.047	0.187	±	0.038	0.254	±	0.043	0.216	±	0.037
	114	0.401	±	0.060	0.302	±	0.045	0.226	±	0.037	0.252	±	0.041	0.286	±	0.037
	118	0.422	±	0.058	0.334	±	0.043	0.365	±	0.035	0.322	±	0.039	0.232	±	0.036
	122	0.450	±	0.057	0.417	±	0.041	0.324	±	0.033	0.281	±	0.039	0.228	±	0.033
	126	0.547	±	0.053	0.453	±	0.039	0.337	±	0.032	0.303	±	0.036	0.224	±	0.032
"B"	130	0.481	±	0.050	0.331	±	0.039	0.296	±	0.030	0.303	±	0.034	0.196	±	0.031
	134	0.393	±	0.050	0.379	±	0.064	0.346	±	0.029	0.328	±	0.032	0.207	±	0.028
	138	0.395	±	0.050	0.317	±	0.035	0.318	±	0.028	0.271	±	0.031	0.229	±	0.026
	142	0.354	±	0.050	0.324	±	0.035	0.238	±	0.027	0.171	±	0.030	0.172	±	0.024
	146	0.298	±	0.054	0.290	±	0.035	0.236	±	0.027	0.170	±	0.029	0.143	±	0.024
	150	0.318	±	0.060	0.131	±	0.039	0.154	±	0.028	0.094	±	0.029	0.046	±	0.024
	154	-0.003	±	0.063	0.030	±	0.044	0.028	±	0.031	-0.049	±	0.031	-0.032	±	0.026
	158	-0.088	±	0.072	0.004	±	0.047	-0.100	±	0.036	-0.088	±	0.035	-0.157	±	0.032
	162	-0.454	±	0.150	-0.172	±	0.094	-0.120	±	0.079	-0.198	±	0.098	-0.039	±	0.117

from the comparison of results obtained for the two target halves. The fact that the upper part has a larger polarization than the lower half can be due to the fact that the microwaves were injected from above and that there is absorption in the target material.

4) A vertical target polarization component coming either from a misalignment of the saddle coil or an imperfect 90° turn of the magnetic field in the adiabatic rotation were ruled out.

With other configurations of the beam/target polarization orientations, it is not possible to measure one spin-parameter alone. For the vertical target and beam polarization orientations, it was possible to do a similar analysis as for A_{ookk} assuming A_{oono} to be known; A^+_{oonn} and A^-_{oonn} were found consistent. For the (x,xz) target orienta-

tion, it was possible to compare A^+_{oopq} and A^-_{oopq}. Again a 12% relative disagreement was found. This also has not been explained. As a consequence, all results obtained with a longitudinally polarized target should include a multiplicative uncertainty of ±6%.

The uncertainties of the beam polarization P_B and target polarization P_T, lead to multiplicative systematic errors. Beam polarization values used in the analysis have been calculated using an ad hoc function fitting the experimental data [9]. Relative errors $\Delta P_B/P_B$ vary from 1 to 3% depending on the incident neutron energy. The target polarization was measured with a relative precision between 3 and 4% (see Sect. 2.2). The estimated relative uncertainties for the spin-correlation parameters as a function of the beam energy, obtained by adding these two

Table 5. Numerical values for the np elastic scattering spin-correlation observable A_{ookk} as a function of $\Theta_{c.m.}$ and the neutron kinetic energy. The errors are purely statistical. To obtain the normalization errors one must include an extra 6% uncertainty to the ones given in Table 2b)

$\Theta_{c.m.}$ [°]	260 MeV	315 MeV	380 MeV	460 MeV	535 MeV
58					0.037 ± 0.028
62				0.001 ± 0.068	0.047 ± 0.013
66				0.048 ± 0.021	0.088 ± 0.012
70			0.076 ± 0.035	0.084 ± 0.016	0.139 ± 0.013
74			0.126 ± 0.020	0.135 ± 0.016	0.181 ± 0.013
78		0.315 ± 0.057	0.222 ± 0.017	0.149 ± 0.016	0.215 ± 0.013
82		0.293 ± 0.027	0.262 ± 0.016	0.227 ± 0.016	0.264 ± 0.014
"A" 86	0.447 ± 0.141	0.413 ± 0.022	0.290 ± 0.016	0.301 ± 0.016	0.279 ± 0.014
90	0.600 ± 0.044	0.453 ± 0.020	0.442 ± 0.016	0.384 ± 0.017	0.338 ± 0.014
94	0.612 ± 0.031	0.514 ± 0.019	0.485 ± 0.015	0.422 ± 0.016	0.381 ± 0.014
98	0.692 ± 0.027	0.604 ± 0.019	0.594 ± 0.015	0.490 ± 0.016	0.422 ± 0.014
102	0.780 ± 0.025	0.677 ± 0.018	0.635 ± 0.015	0.561 ± 0.016	0.476 ± 0.014
106	0.793 ± 0.024	0.725 ± 0.017	0.669 ± 0.014	0.620 ± 0.016	0.534 ± 0.015
110	0.765 ± 0.023	0.716 ± 0.017	0.763 ± 0.014	0.713 ± 0.015	0.590 ± 0.014
114	0.785 ± 0.022	0.737 ± 0.016	0.756 ± 0.014	0.734 ± 0.015	0.636 ± 0.014
118	0.736 ± 0.028	0.728 ± 0.019	0.769 ± 0.015	0.742 ± 0.017	0.617 ± 0.019
102	0.786 ± 0.045	0.788 ± 0.036	0.641 ± 0.039	0.451 ± 0.067	0.476 ± 0.098
106	0.778 ± 0.029	0.721 ± 0.020	0.688 ± 0.017	0.653 ± 0.021	0.533 ± 0.020
110	0.757 ± 0.027	0.716 ± 0.019	0.755 ± 0.016	0.697 ± 0.018	0.566 ± 0.016
114	0.705 ± 0.026	0.740 ± 0.019	0.744 ± 0.016	0.791 ± 0.017	0.612 ± 0.016
118	0.749 ± 0.025	0.707 ± 0.018	0.740 ± 0.015	0.776 ± 0.017	0.635 ± 0.015
122	0.680 ± 0.023	0.685 ± 0.017	0.707 ± 0.014	0.796 ± 0.016	0.687 ± 0.015
126	0.686 ± 0.022	0.647 ± 0.016	0.697 ± 0.014	0.748 ± 0.016	0.660 ± 0.014
"B" 130	0.608 ± 0.022	0.597 ± 0.016	0.641 ± 0.013	0.717 ± 0.015	0.678 ± 0.013
134	0.490 ± 0.022	0.561 ± 0.015	0.616 ± 0.013	0.685 ± 0.014	0.634 ± 0.012
138	0.489 ± 0.021	0.457 ± 0.015	0.546 ± 0.012	0.624 ± 0.013	0.605 ± 0.012
142	0.419 ± 0.021	0.417 ± 0.015	0.457 ± 0.012	0.531 ± 0.013	0.521 ± 0.011
146	0.319 ± 0.023	0.334 ± 0.015	0.363 ± 0.012	0.439 ± 0.013	0.440 ± 0.011
150	0.217 ± 0.025	0.231 ± 0.017	0.264 ± 0.012	0.333 ± 0.012	0.351 ± 0.011
154	0.069 ± 0.027	0.076 ± 0.018	0.137 ± 0.014	0.192 ± 0.013	0.213 ± 0.011
158	-0.078 ± 0.030	-0.067 ± 0.020	-0.046 ± 0.015	-0.033 ± 0.015	0.093 ± 0.013
162	-0.233 ± 0.052	-0.213 ± 0.032	-0.243 ± 0.024	-0.157 ± 0.024	-0.089 ± 0.022

contributions in quadrature are listed in Table 2b). These normalization factors apply to the data taken with the vertically polarized target, i.e A_{oonn}. For the other spin-correlation parameters taken with a longitudinally polarized target, one should include the extra ±6% uncertainty as mentioned above.

5 Results and discussions

Results are given as a function of the c.m. scattering angle ($\Theta_{c.m.}$) for five energies, namely 260, 315, 380, 460 and 535 MeV. These energies correspond to the central values of five energy bins covering the intervals 230–290, 290–340, 340–420, 420–500 and 500–570 MeV, respectively. Numerical values for the analyzing power A_{oono} are given in

Table 3 and Tables 4 and 5 contain the results for the spin-correlation parameters, A_{oonn} and A_{ookk}, measured without any parasitic spin components. Numerical values for the A_{oopq} parameters measured as a linear combination of the A_{ookk}, A_{oosk} and A_{ooss} parameters in position $(\mathbf{x}, \mathbf{xz})$ are given in Table 6, those for the A_{oopq} measured as a linear combination of A_{ookk}, A_{oosk} in position $(\mathbf{x}, \mathbf{z})$ are given in Table 7. The coefficients of the linear combinations are energy dependent as indicated in Table 1. The error on the data reflect the statistical uncertainty.

The A_{oono} results are displayed in Fig. 6 and the four pure spin correlation observables in Fig. 7 as functions of $\Theta_{c.m.}$ for the five energy bins. Here we chose to show the pure correlation parameters A_{oosk} and A_{ooss} instead of their linear combinations to ease the comparison with the-

Table 6. Numerical values for the np elastic scattering spin observable A_{oopq} measured in the $(\mathbf{x}, \mathbf{xz})$ position as a linear combination of A_{ooss}, A_{oosk} and A_{ookk} (see Table 1). The errors are purely statistical. To obtain the normalization errors one must include an extra 6% uncertainty to the ones given in Table 2b)

	$\Theta_{c.m.}$ [°]	260 MeV	315 MeV	380 MeV	460 MeV	535 MeV
	58					-0.056 ± 0.037
	62				-0.147 ± 0.102	-0.066 ± 0.018
	66				-0.074 ± 0.032	-0.055 ± 0.018
	70			-0.028 ± 0.051	-0.036 ± 0.024	-0.081 ± 0.018
	74			-0.016 ± 0.029	-0.015 ± 0.024	-0.051 ± 0.018
	78		-0.035 ± 0.084	0.004 ± 0.024	-0.011 ± 0.024	-0.030 ± 0.019
	82		0.100 ± 0.040	0.043 ± 0.023	0.024 ± 0.024	-0.014 ± 0.019
"A"	86	0.209 ± 0.216	0.105 ± 0.032	0.079 ± 0.023	0.113 ± 0.024	0.051 ± 0.019
	90	0.179 ± 0.066	0.131 ± 0.030	0.135 ± 0.023	0.103 ± 0.024	0.093 ± 0.019
	94	0.331 ± 0.045	0.173 ± 0.028	0.183 ± 0.022	0.176 ± 0.023	0.123 ± 0.019
	98	0.237 ± 0.041	0.239 ± 0.026	0.178 ± 0.021	0.237 ± 0.022	0.205 ± 0.019
	102	0.359 ± 0.038	0.261 ± 0.025	0.230 ± 0.020	0.248 ± 0.022	0.251 ± 0.019
	106	0.364 ± 0.035	0.291 ± 0.024	0.251 ± 0.020	0.264 ± 0.021	0.310 ± 0.019
	110	0.412 ± 0.033	0.336 ± 0.023	0.259 ± 0.019	0.305 ± 0.020	0.298 ± 0.019
	114	0.408 ± 0.031	0.303 ± 0.022	0.266 ± 0.018	0.288 ± 0.020	0.283 ± 0.019
	118	0.437 ± 0.043	0.336 ± 0.027	0.254 ± 0.021	0.259 ± 0.023	0.300 ± 0.025
	102	0.353 ± 0.067	0.289 ± 0.050	0.325 ± 0.050	0.487 ± 0.086	0.040 ± 0.106
	106	0.424 ± 0.044	0.279 ± 0.030	0.264 ± 0.024	0.256 ± 0.029	0.251 ± 0.026
	110	0.372 ± 0.041	0.287 ± 0.028	0.217 ± 0.023	0.311 ± 0.026	0.320 ± 0.021
	114	0.386 ± 0.038	0.313 ± 0.027	0.261 ± 0.022	0.283 ± 0.025	0.323 ± 0.021
	118	0.476 ± 0.035	0.310 ± 0.025	0.301 ± 0.021	0.329 ± 0.024	0.307 ± 0.020
	122	0.463 ± 0.033	0.372 ± 0.023	0.285 ± 0.020	0.271 ± 0.022	0.268 ± 0.020
	126	0.476 ± 0.031	0.336 ± 0.022	0.321 ± 0.018	0.278 ± 0.021	0.231 ± 0.018
"B"	130	0.494 ± 0.029	0.362 ± 0.021	0.290 ± 0.017	0.218 ± 0.019	0.192 ± 0.017
	134	0.481 ± 0.028	0.427 ± 0.019	0.369 ± 0.016	0.267 ± 0.018	0.168 ± 0.015
	138	0.537 ± 0.027	0.404 ± 0.019	0.353 ± 0.015	0.258 ± 0.017	0.204 ± 0.015
	142	0.535 ± 0.027	0.458 ± 0.018	0.385 ± 0.015	0.295 ± 0.016	0.229 ± 0.013
	146	0.545 ± 0.028	0.497 ± 0.019	0.431 ± 0.014	0.347 ± 0.015	0.223 ± 0.013
	150	0.598 ± 0.030	0.509 ± 0.020	0.463 ± 0.015	0.385 ± 0.015	0.276 ± 0.013
	154	0.610 ± 0.031	0.551 ± 0.021	0.543 ± 0.016	0.463 ± 0.016	0.356 ± 0.013
	158	0.613 ± 0.035	0.556 ± 0.022	0.591 ± 0.016	0.533 ± 0.017	0.433 ± 0.014
	162	0.594 ± 0.059	0.644 ± 0.035	0.599 ± 0.025	0.556 ± 0.026	0.495 ± 0.024

oretical predictions. The angular range was covered with two detector arm positions, and the corresponding results are shown by full dots (position "A") and open circles (position "B"). The overlapping points are generally in very good agreement with each other. Only the A_{oosk} data show, at low energy, incompatibility between the data of the two angular positions. It could be due to the fact that, in the $(\mathbf{x}, \mathbf{z})$ configuration, even though the coefficient in front of A_{oosk} is almost 1, the contribution from A_{ookk} is dominant and a small error on its coefficient reflects heavily on A_{oosk}. After many tests, no answer has been found to explain this disagreement.

In each plot, four phenomenological predictions of spin observables are shown (none of these predictions contains the present data): solid lines and dashed lines correspond to the phase shift solutions from the Saclay-Geneva analysis [15] and from R.Arndt (VPI PSA) [16], respectively. Two predictions obtained by potential model calculations are also presented; the dotted line corresponds to the Paris potential [17] and the dashed-dotted one to the Bonn potential [18].

In Fig. 6 showing the analyzing power, it is almost impossible to distinguish among the four predictions. On the other hand, in Fig. 7, the main disagreement is seen for the A_{oonn} parameter: the Paris potential model predicts very small values compared to the PSA predictions, which also disagree significantly from each other eventhough containing the same data base. Such a strong disagreement is rather surprising for a parameter which has been abundantly measured [19–22]. Table 8 summarizes the other

Table 7. Numerical values for the np elastic scattering spin observable A_{oopq} measured in the $(\mathbf{x}, \mathbf{z})$ position as a linear combination of A_{oosk} and A_{ookk} (see Table 1). The errors are purely statistical. To obtain the normalization factors one must include an extra 6% uncertainty to the ones given in Table 2b)

	$\Theta_{c.m.}$ [°]	260 MeV	315 MeV	380 MeV	460 MeV	535 MeV
	58					0.106 ± 0.029
	62				0.013 ± 0.056	0.018 ± 0.012
	66				0.023 ± 0.019	0.008 ± 0.011
	70			-0.052 ± 0.033	-0.020 ± 0.015	0.014 ± 0.012
	74			-0.008 ± 0.018	-0.029 ± 0.015	-0.014 ± 0.012
	78		-0.032 ± 0.053	-0.034 ± 0.016	-0.027 ± 0.016	-0.023 ± 0.013
	82		-0.025 ± 0.026	-0.017 ± 0.015	-0.029 ± 0.016	0.002 ± 0.013
"A"	86	0.111 ± 0.133	0.004 ± 0.020	-0.033 ± 0.015	-0.026 ± 0.016	-0.038 ± 0.013
	90	0.043 ± 0.041	-0.009 ± 0.019	0.002 ± 0.015	-0.023 ± 0.016	-0.013 ± 0.013
	94	0.062 ± 0.029	0.026 ± 0.018	-0.012 ± 0.015	0.021 ± 0.016	-0.013 ± 0.014
	98	0.064 ± 0.025	0.040 ± 0.018	0.025 ± 0.015	0.038 ± 0.016	0.000 ± 0.014
	102	0.079 ± 0.025	0.051 ± 0.018	0.034 ± 0.015	0.035 ± 0.016	0.009 ± 0.014
	106	0.133 ± 0.024	0.072 ± 0.017	0.053 ± 0.015	0.084 ± 0.016	0.030 ± 0.015
	110	0.121 ± 0.023	0.063 ± 0.017	0.040 ± 0.014	0.039 ± 0.016	0.069 ± 0.015
	114	0.094 ± 0.022	0.065 ± 0.017	0.069 ± 0.015	0.079 ± 0.019	0.059 ± 0.021
	118	0.081 ± 0.047	0.048 ± 0.040	0.177 ± 0.046	-0.138 ± 0.094	-0.332 ± 0.212
	102	0.149 ± 0.045	0.145 ± 0.035	0.139 ± 0.039	-0.086 ± 0.065	0.057 ± 0.094
	106	0.184 ± 0.029	0.102 ± 0.020	0.088 ± 0.017	0.071 ± 0.020	0.081 ± 0.020
	110	0.101 ± 0.027	0.144 ± 0.019	0.050 ± 0.016	0.064 ± 0.018	0.089 ± 0.016
	114	0.161 ± 0.026	0.140 ± 0.018	0.088 ± 0.016	0.084 ± 0.017	0.061 ± 0.016
	118	0.088 ± 0.024	0.110 ± 0.018	0.062 ± 0.015	0.063 ± 0.017	0.063 ± 0.015
	122	0.149 ± 0.023	0.118 ± 0.017	0.052 ± 0.014	0.056 ± 0.016	0.036 ± 0.015
	126	0.116 ± 0.022	0.084 ± 0.016	0.050 ± 0.014	0.073 ± 0.016	0.088 ± 0.014
"B"	130	0.095 ± 0.021	0.069 ± 0.016	0.018 ± 0.013	0.022 ± 0.015	0.035 ± 0.013
	134	0.061 ± 0.021	0.064 ± 0.015	0.017 ± 0.013	-0.050 ± 0.014	0.033 ± 0.012
	138	0.034 ± 0.021	0.021 ± 0.015	-0.009 ± 0.012	-0.019 ± 0.013	0.010 ± 0.012
	142	0.059 ± 0.021	-0.010 ± 0.015	-0.026 ± 0.012	-0.026 ± 0.013	0.006 ± 0.011
	146	0.012 ± 0.023	-0.031 ± 0.015	-0.042 ± 0.012	-0.044 ± 0.013	-0.038 ± 0.011
	150	-0.022 ± 0.025	-0.055 ± 0.016	-0.056 ± 0.012	-0.096 ± 0.012	-0.043 ± 0.011
	154	-0.091 ± 0.026	-0.074 ± 0.018	-0.083 ± 0.014	-0.075 ± 0.013	-0.054 ± 0.011
	158	-0.087 ± 0.030	-0.089 ± 0.020	-0.129 ± 0.015	-0.059 ± 0.015	-0.041 ± 0.013
	162	-0.201 ± 0.051	-0.175 ± 0.032	-0.115 ± 0.023	-0.051 ± 0.024	-0.040 ± 0.022

Table 8. Data from other experiments on the spin correlation parameters in the energy range 200-600 MeV

	lab [ref]	energy	points	angular range	typical errors
A_{oonn}	LAMPF '81 [21]	395 MeV	15	72° - 166°	0.08
		465 MeV	15	70° - 166°	0.07
		565 MeV	15	70° - 166°	0.12
	TRIUMF '89 [19]	220 MeV	16	71° - 144°	0.02
		325 MeV	19	62° - 146°	0.02
		425 MeV	19	52° - 143°	0.03
	LAMPF '96 [20]	484 MeV	5	155° - 175°	0.15
A_{ooss}	LAMPF '96 [20]	484 MeV	31	25° - 175°	0.18
A_{ookk}	LAMPF '96 [20]	484 MeV	29	40° - 179°	0.08
	Saturne '94 [22]	312 MeV	11	50° - 90°	0.13
A_{oosk}	LAMPF '96 [20]	484 MeV	31	25° - 175°	0.09

available data on the spin correlation parameters measured in the energy range 200-600 MeV. These correlation data [19–22] are not shown on Fig. 7 as they have not been measured at the same energies. For what concerns the A_{oonn} parameter, we found that the disagreement between the two PSA predictions comes from the fact that, in the VPI PSA, a large multiplicative normalization factor of ~ 1.20 is applied on the TRIUMF data [19], a normalization value well above the one of 5% recommended by the authors. Our data are in excellent agreement with the TRIUMF data [19] indicating that the TRIUMF data should not be largely normalized.

As much as the three other correlation parameters measured with the longitudinal polarized target are concerned, one observes that our results lie below the PSA and potential predictions, which is most striking on the A_{ookk} parameter. We checked whether the PSA predictions could be altered by the introduction of these data: it was found, using the Saclay-Geneva PSA, that no fit could be obtained without applying a $\sim10\%$ normalization factor on the data. We also reached a similar conclusion when trying to do a direct amplitude reconstruction of the np amplitudes: without normalization we reached parasitic minima providing strange behaviour of one of the scattering amplitudes. This confirms the assessment of a $\pm6\%$ error for the target polarization uncertainties as discussed in Sect. 4.5.

These results should encourage theoreticians to improve their models in order to better reproduce these new data. They will also help to stabilize the solutions in PSA analyses. When combined with other data from LAMPF and TRIUMF, it is anticipated that the knowledge of the $I = 0$ nucleon-nucleon amplitudes will be greatly improved compared to several years ago.

References

1. R. Hausammann et al., Phys. Rev. Lett. **46**, 1047 (1981)
2. C. Lechanoine-Leluc and F. Lehar, Rev. Mod. Phys **65**, 1 (1993) and SPIN98, Protvino; 13th International Symposium on High Energy Spin Physics, edited by N.E.Tyurin, V.L.Solovianov, S.M.Troshin, A.G. Ufimtsev, World Scientific, page 356 (1999)
3. J. Bystricky, F. Lehar and P.Winternitz, J. Phys. (Paris) **39**, 1 (1978)
4. A. Teglia, PhD thesis, Univ. of Geneva, (1997) No. 2948
5. J. Arnold et al., see the same issue of Eur. Phys. J. C
6. A. Ahmidouch et al., Eur. Phys. J. C **2**, 627 (1998)
7. J. Arnold et al., Nucl. Instrum. Methods A **386**, 211 (1997)
8. R. Binz et al., Phys. Lett. B **231**, 323 (1989)
9. J. Arnold et al., Eur. Phys. J. A **2**, 411 (1998)
10. Ch. Brönnimann et al., Nucl. Instrum. Methods A **343**, 331 (1994)
11. B. van den Brandt et al., Nucl. Instrum. Methods A **356**, 53 (1995)
12. D. Besset et al., Nucl. Instrum. Methods **184**, 365 (1981)
13. A. Ahmidouch et al., Nucl. Instrum. Methods A **326**, 538 (1993)
14. Basle convention, Nucl. Phys. **21**, 698 (1960)
15. J. Bystricky et al. J. Phys. (France) **48**, 199 (1987) and private communication
16. R.A.Arndt et al., SAID - Scattering Analyses Interactive xial-In,
   WWW-address: http://clsaid.phys.vt.edu/~CAPS/
17. M. Lacombe et al., Phys. Rev. C **21**, 861 (1988) and Phys. Rev. D **12**, 1495 (1975)
18. R. Machleidt et al., Mesons In Nuclei, Vol 1, Amsterdam, 1979 and C. Elster et al., Phys. Rev. C **37**, 1647 (1998) and Phys. Rev. C **38**, 1828 (1988)
19. D. Bandyopadhyay et al., Phys. Rev. C **40**, 2684 (1989)
20. V. Carlson et al., Phys. Rev. D **53**, 3586 (1996) see also Phys. Rev. Lett. **59**, 1645 (1987) and Phys. Rev. D **40**, 1788 (1989) and Phys. Rev. D **46**, 2792 (1992) and Phys. Rev. D **47**, 2 (1993)
21. T.S. Bhatia et al., Polarisation Phenomena In Nuclear Physics, AIP Conference Proceedings 69, (1981), 123–125, Santa Fe 1980
22. J. Ball et al., Nucl. Phys. A **574**, 697 (1994)